Sensors and Materials, Vol. 37, No. 3 (2025) 1243–1258
MYU Tokyo

S & M 3984

Diagnosis of Wind Turbine Gearbox Using Artificial Intelligence of Things with Extension Detection Method

Meng-Hui Wang, Yu-Xian Su, and Shiue-Der Lu*

Department of Electrical Engineering, National Chin-Yi University of Technology,
No. 57, Sec. 2, Zhongshan Rd., Taiping Dist., Taichung 411030, Taiwan (R.O.C.)

(Received June 30, 2024; accepted February 21, 2025)

Keywords: extension, fast Fourier transform, correlation function, wind turbines

Wind energy does not produce air or water pollution during its generation and is one of the fastest-growing energy sources worldwide. As a result, the demand for efficient wind turbine operation is increasing, and the condition of the gearbox significantly affects the operation of the entire wind turbine. In this article, we propose using extension theory for the fault identification of the gearbox. Owing to the characteristics of extension sets, where the feature values range from $-\infty$ to $+\infty$, compared with fuzzy sets with values ranging from 0 to 1, extension sets are more convenient than fuzzy sets for quantifying feature values. Therefore, we selected extension theory as the basis for the experiment. For subsequent analysis, a model with four gears and a low speed-to-high speed ratio of 1:12.25 was constructed on the basis of the structure of large wind turbines. A servo motor was used to simulate the operation driven by wind-transmitted energy, and an NI-9234 high-speed acquisition card, along with a three-axis vibration sensor, was used to collect the generated data. The collected vibration signals were processed using fast Fourier transform to reduce unnecessary noise. The signals were categorized into different range intervals on the basis of vibration amplitude, and the occurrences of each interval were used as features for classification. Matrix Laboratory was employed to calculate the correlation function values to determine the fault types. Experimental results showed that the proposed method achieved a recognition success rate of 94.625% for four different types of gearbox. Thus, by this method, we effectively classified gearboxes and achieved the goal of gearbox fault diagnosis.

1. Introduction

In recent years, with the continuous advancement of global technology, the demand for energy has steadily increased. The concept of environmental protection was consistently emphasized, prompting renewable energy to become a key focus in the development of power systems. Particularly in countries with abundant wind resources, wind power development was rapid.[1,2] However, whether offshore or onshore, wind turbines are exposed to harsh environmental conditions. Over time, this increased the likelihood of component wear and aging, posing significant challenges for the maintenance and fault diagnosis of wind turbines.

*Corresponding author: e-mail: sdl@ncut.edu.tw
https://doi.org/10.18494/SAM5225

ISSN 0914-4935

According to historical data, gearbox failures account for 60% of wind turbine transmission system failures.[3] Previously, gearbox fault diagnosis methods included temperature measurement analysis, vibration analysis, acoustic measurement, and oil sample analysis, among others. Vibration signals, in particular, were widely used in fault diagnosis because they contained a wealth of detailed fault information.[4–10]

Extension sets, which describe feature values in the range of $-\infty$ to $+\infty$, were more convenient for quantifying feature values than the fuzzy set range of 0 to 1. Extension theory was used to solve many problems.[11] For example, Zeng *et al.* used it for a Wildfire Risk Assessment Model for Transmission Lines.[12] Wu *et al.* used it to evaluate power grid technology renovation projects.[13] Zhao *et al.* implemented a Predictive Method for Weak Signal Evolution.[14] Liu *et al.* used it for the Configuration of Product Plans.[15] Chen *et al.* used it for Risk Assessment Methods of Power Communication Networks.[16] These examples demonstrated the potential of extension theory. In this article, we propose using vibration signals from wind turbine gearboxes, combined with the correlation function calculation of extension, to determine the fault modes of these signals.

2. Literature Review

In conventional approaches, signal processing outcomes for unknown health states are compared with those from normal health conditions to detect faults. Typical techniques include Fourier spectral analysis, empirical mode decomposition, wavelet analysis, and cepstrum analysis.[17]

Traditional methods were not well-suited for handling large and complex signals. As a result, intelligent fault diagnosis methods gained increasing attention for their ability to overcome these limitations of traditional approaches.[18]

Amin *et al.* introduced two methods: a cyclostationary-based convolutional neural network (CNN) and a kurtogram-based CNN. These techniques effectively identified faults in low-speed shafts and evaluated the severity of the faults through simulation analyses, achieving accuracy rates of 87 and 81.5%, respectively.[19]

He *et al.* developed a deep learning algorithm called the dilated CNN (DCNN) for detecting faults in wind turbine gearboxes. Unlike traditional CNNs, DCNN employs dilated convolution rather than standard convolution, allowing each operation to capture information over a range of input data wider than that in the case of standard convolution.[20]

Zhang *et al.* presented a novel fault diagnosis approach that integrates optimized singular value decomposition (SVD), symmetrized dot patterns (SDPs), and CNN, known as the SVD–SDP–CNN method.[21]

In this paper, we propose an extended detection method for the fault diagnosis of wind turbines. This method does not require converting data into images; it only requires filtering before recognition can begin, saving significant time. The accuracy reached 94.625%, making it highly effective for the fault diagnosis of the gearbox in wind turbines.

3. Research Framework and Model Design

3.1 Wind turbine fault identification system architecture

The rotational system of the wind turbine, consisting of a servo motor, gearbox, and generator, was used as the platform for signal collection in this study. Data were transmitted to a computer for analysis via a three-axis vibration sensor and an NI-9234 acquisition card. After filtering out unwanted signals using fast Fourier transform (FFT), the necessary features were extracted. The fault results were then obtained through the calculation of extension correlation functions. The experimental setup is shown in Fig. 1, and the specifications of the equipment are shown in Table 1.

3.2 Design of a wind turbine gearbox

Owing to the wind turbine's rotational speed being unable to meet the requirements for starting the generator, a gearbox was needed to increase the speed, allowing the generator to operate at its rated speed. In this study, we used four types of gearbox to simulate faults.

3.2.1 Gearbox I (standard model)

We designed a standard model based on the structure of large wind turbines, comprising four normal gears. The ratio of the low-speed shaft to the high-speed shaft is 1:12.25, with HD220 lubricant being used. The internal configuration is illustrated in Fig. 2(a), whereas Fig. 2(b) depicts the physical model. Table 2 outlines the number of teeth for each gear.

3.2.2 Gearbox II (gear rust)

Wind turbines are typically installed outdoors, exposed to humid climates. If the gearbox lacks proper sealing or is exposed to moisture, water and oxygen can come into contact with the

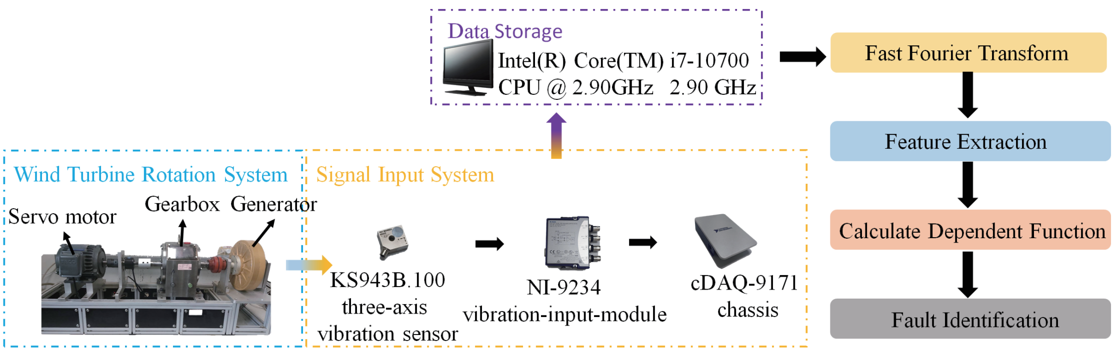

Fig. 1. (Color online) Experimental architecture diagram.

Table 1
Detailed specifications of the components for the wind turbine test platform.

Number	Figure	Specification
(1)	NI-9234 DAQ	32-bit resolution, 4 synchronous channels, 51.2 kHz
(2)	There-axis vibration sensor (voltage sensitivity)	Sensitivity of 100% ± 5 (mV/g)
(3)	Gearbox	Gear ratio of 1 to 12.25
(4)	Induction motor	1.5 hp

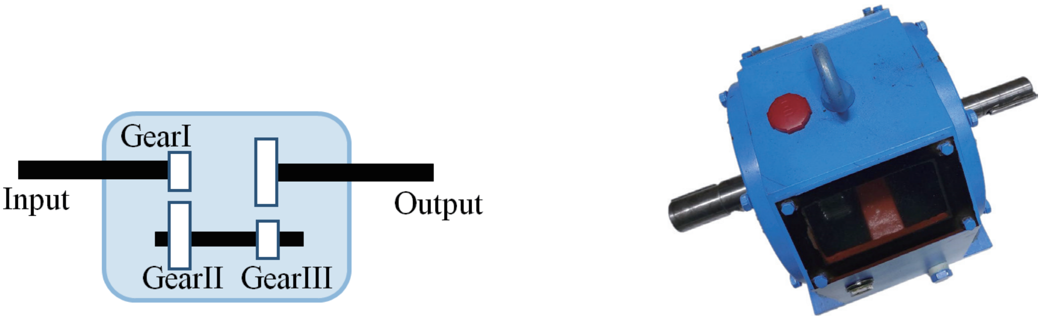

(a) (b)

Fig. 2. (Color online) Gearbox Model I: (a) internal structure diagram and (b) gearbox physical diagram.

Table 2
Gear specifications of gearbox.

Type	Numbers of gear teeth
Gear I	14
Gear II	49
Gear III	14
Gear IV	49

metal surfaces, leading to gear rusting. In this study, we used rusted gears to simulate this scenario, as shown in Fig. 3.

3.2.3 Gearbox III (gear surface fracture)

During prolonged operation, gears develop cracks or fractures due to material fatigue, or they experience surface fractures because of extended loads exceeding their design capacity or sudden overloads. In this study, we simulated these conditions by damaging the gears, as shown in Fig. 4.

3.2.4 Gearbox IV (gear surface wear)

When the lubricating oil quality is poor, many particles cause wear on the internal gears of the gearbox during operation. To simulate this condition, we subjected four gears to wear, as shown in Fig. 5.

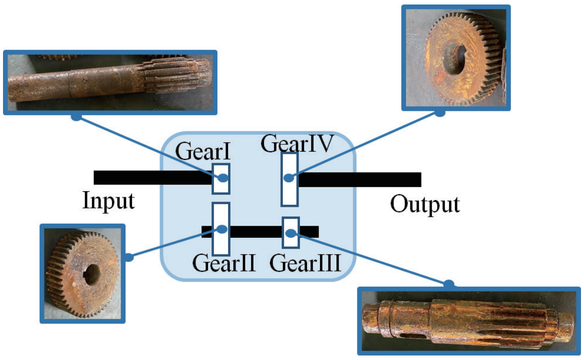

Fig. 3. (Color online) Gearbox Model II.

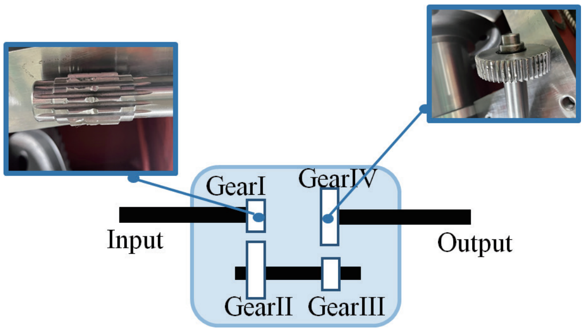

Fig. 4. (Color online) Gearbox Model III.

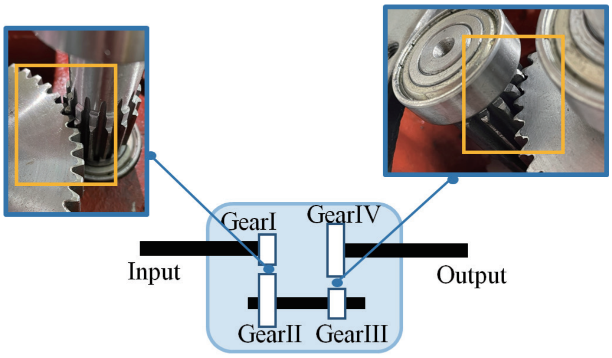

Fig. 5. (Color online) Gearbox Model IV.

4. Method

4.1 FFT

During the process of measuring vibration signals in wind turbines, interference from the surrounding environment and electrical equipment was frequently encountered. To improve fault detection accuracy, a band-pass filter was used to eliminate interference below 60 Hz and minor noise above 15 kHz. This ensured that the frequency signals in the 60 Hz to 15 kHz range were retained more clearly. In this study, the original signals were processed using FFT to convert them from the time domain to the frequency domain. As shown in Figs. 6(a) and 6(b), the blue rectangular areas represent subtle noise above 15 kHz, where it can be seen in the figure that the signal in this region was clearly filtered out.

4.2 Extension theory

The extension theory, introduced by Professor Wen Cai in 1983, offers a novel approach to address incompatible and contradictory issues. This theory mainly comprises two parts: Object

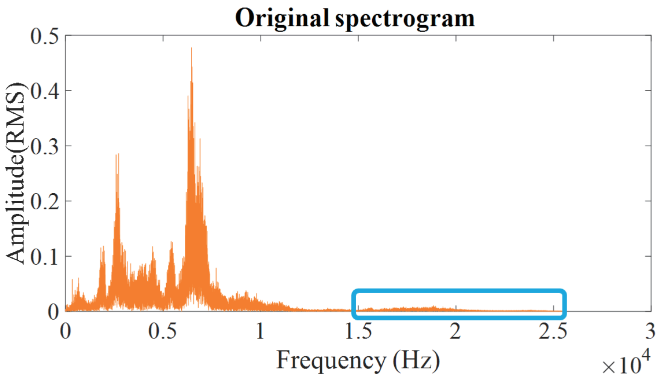

(a)

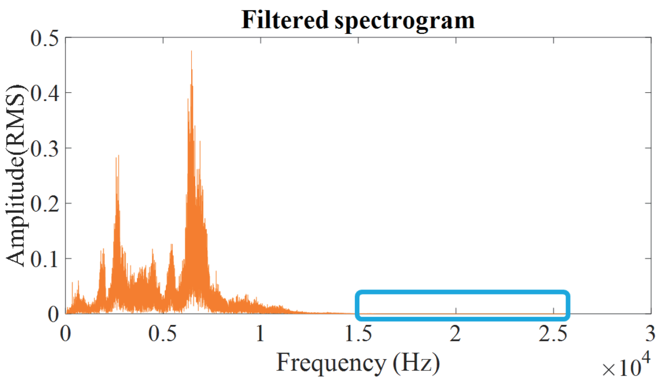

(b)

Fig. 6. (Color online) FFT: (a) before and (b) after filtering.

Element Theory and Extension Mathematics. Extension Mathematics utilizes extension sets and extension correlation functions as primary tools, replacing the explicit sets in traditional mathematics. Object Element Theory decomposes objects into the scope values of characteristics and characteristic extensions. By transforming object relationships, we can evaluate the impact of each characteristic on objects and understand their importance. Extension Theory describes the characteristics of objects, transforming discontinuous explicit sets into continuous multivalued sets, and describes the positive and negative degrees and zero boundaries of object characteristics through correlation functions. We used co-correlation functions to describe the positional values of points and intervals in regions and understand the degree of association between elements and the sets of object characteristics through schematic diagrams. The normalized correlation degree ranged from −1 to +1,[22] reflecting the strength of the effect of elements on object characteristics. Overall, Extension Theory provides a powerful framework for handling complex object characteristics and relationships.

4.2.1 Matter-element model

Extension Theory collectively refers to all individuals, events, and objects encountered in daily life as "matter". To distinguish between different matters, the theory assigns unique "matter names" to identify them. Each matter possesses its unique functions, forms, patterns, and relative relationships with other matters, which constitutes the characteristics of matters. These characteristics are associated with characteristic values. Therefore, to provide a comprehensive description of a matter's matter-element model, three fundamental elements are essential: the matter's name, its characteristics, and the corresponding characteristic values.[15,23] The matter-element model, comprising these three elements, can be expressed using a formula. In summary, Extension Theory employs a standardized format to clearly delineate the attributes and values of each matter, as illustrated in Eq. (1).

$$R=\left(N,C,V\right)=\begin{Bmatrix} N & C_1 & \langle V_1\rangle \\ & C_2 & \langle V_2\rangle \\ & \cdots & \cdots \\ & C_n & \langle V_n\rangle \end{Bmatrix} \tag{1}$$

Here, R represents the matter-element, N the matter's name, C the characteristics, V the characteristic values, and n the number of characteristics.

For example, there was a wooden cabinet with a length of 30 cm, a width of 20 cm, and a height of 25 cm. Represented by the matter-element model, the name was "wooden cabinet", and it had three characteristics, namely, length, width, and height, with values of 30, 20, and 25 cm, respectively, as shown in Table 3.

4.2.2 Extension sets

Classical mathematics relies on classical set theory, where the binary numbers 0 and 1 indicate whether an object had a specific attribute. Conversely, fuzzy theory quantifies the degree of uncertainty in attributes within a set using membership functions, with values ranging from 0 to 1. Extension sets go even further by utilizing real numbers spanning from negative to positive infinity to denote the extent to which an object possesses a particular attribute. Simply put, classical mathematics deals with the binary presence or absence of attributes in objects, fuzzy theory addresses the degree of uncertainty in object attributes, and extension sets offer a broad range of representations, showcasing the diversity of attribute degrees.[22]

Table 3
Matter-element model of wooden cabinet.

Name	Characteristics	Characteristic values (cm)
Wooden cabinet	length	30
	width	20
	height	25

4.2.3 Correlation function

The correlation function, also known as the extension distance, is used to show the relative position of a point within a certain interval. This allowed us to understand the degree to which an element belonged to a set of attributes of an object, referred to as the correlation degree. Since the correlation degree varied during calculation, normalization was applied. The maximum value was set to 1, indicating that the element fully conformed to the object's attributes, while a value of −1 indicated complete nonconformity.[23] The normalized correlation degree ranged from −1 to 1, indicating the degree to which an element belonged to or deviated from the characteristics of the object.

Extension transformed the concept of crisp sets in classical mathematics into a continuous multivalued range, which could vary from negative infinity to positive infinity. The correlation function mentioned here was used to quantitatively describe how an element was associated with a specific attribute of an object. Elements could be categorized into a positive domain (representing the degree of conformity), a negative domain (representing nonconformity to the attribute), or a zero boundary (at the edge of the attribute), as shown in Fig. 7.

The classical domain was one specific type of interval, and the universe domain was all types of interval. We defined them as Eq. (2).

$$X_o = \langle a,b \rangle,\ X_p = \langle c,d \rangle,\ X_o \subset X_p. \tag{2}$$

Here, X_o is the classical domain, X_p the universe domain, a the minimum value of the classical domain, b the maximum value of the classical domain, c the minimum value of the universe domain, and d the maximum value of the universe domain. More detailed calculations are provided in Sect. 4.3 (steps 3 to 7).

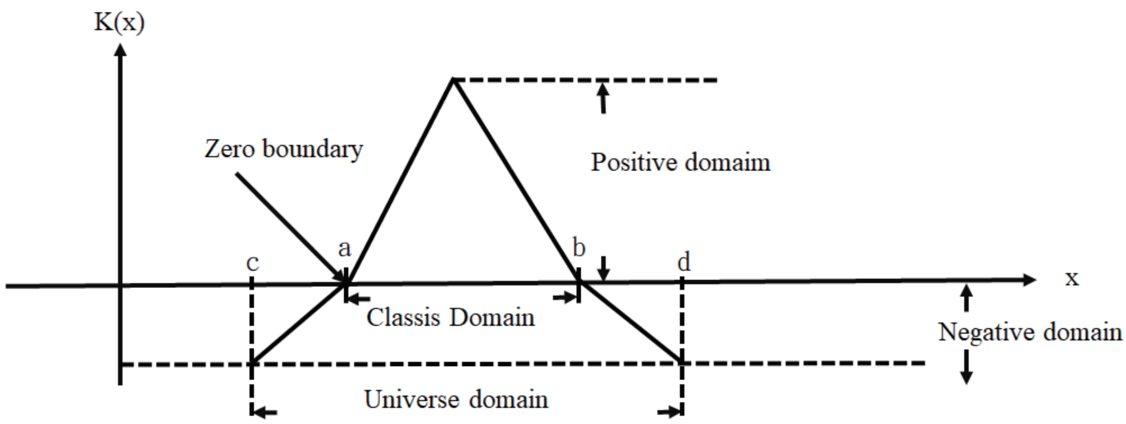

Fig. 7. Correlation function that was used in this study.

4.3 Calculation process by the proposed diagnostic method

Step (1): Define the universe domain and the range of classical domains for different types.

To utilize the extension detection method for distinguishing between different types of signal, defining the matter-element model is necessary, as shown in Eq. (3).

$$R_k=\left(N_k,C_i,X_{ki}\right)=\begin{Bmatrix} N_k & c_1 & \left\langle m_{k1},l_{k1}\right\rangle \\ & c_2 & \left\langle m_{k2},l_{k2}\right\rangle \\ & \cdots & \cdots \\ & c_{12} & \left\langle m_{k12},l_{k12}\right\rangle \end{Bmatrix} \tag{3}$$

Here, R_k represents the matter-element of the kth type, N_k the name of the kth matter-element (k = 1, 2, ..., 4), C_i the ith characteristic within the matter-element (i = 1, 2, ..., 12), X_{ki} the classical domain range of the ith characteristic within the kth category, m_{ki} the minimum characteristic value of the ith feature within the kth category of matter-elements, and l_{ki} the maximum characteristic value of the ith feature within the kth category of matter-elements.

We integrate all classical domains into a universe domain of extension, representing the range of characteristic values within all types of classical domain used in this article, as shown in Eq. (4).

$$R_p=\left(N_p,C_i,X_{pi}\right)=\begin{Bmatrix} N_p & c_1 & \left\langle m_{p1},l_{p1}\right\rangle \\ & c_2 & \left\langle m_{p2},l_{p2}\right\rangle \\ & \cdots & \cdots \\ & c_{12} & \left\langle m_{pi},l_{p12}\right\rangle \end{Bmatrix} \tag{4}$$

Here, R_p represents the universe domain composed of all classical domains, m_{pi} the minimum characteristic value of the ith characteristic within the universe domain, and l_{pi} the maximum characteristic value of the ith characteristic within the universe domain.

We used vibration signals as the name of the matter-element model. The x-axis and y-axis vibration amplitudes of the signals were each divided into five intervals, and the peak-to-peak values of the two axes formed twelve characteristics of this signal. Table 4 shows the matter-element model of gearbox I.

Step (2): Set the weighting values.

The weighting coefficients of the extension detection method are set on the basis of the importance of features, as shown in Eq. (5).

$$\sum_{j=1}^{12}\omega_j=1 \tag{5}$$

Here, ω_j represents the weighting value of the extension detection method.

Table 4
Matter-element model of gearbox I.

Name	Characteristics	Characteristic values
Wooden cabinet	X-axis peak-to-peak	<V1min,V1max>
	Y-axis peak-to-peak	<V2min,V2max>
	Number of points on the X-axis that are between 10g and 20g	<V3min,V3max>
	Number of points on the X-axis that are between 20g and 30g	<V4min,V4max>
	Number of points on the X-axis that are between 30g and 40g	<V5min,V5max>
	Number of points on the X-axis that are between 40g and 50g	<V6min,V6max>
	Number of points on the X-axis greater than 50g	<V7min,V7max>
	Number of points on the Y-axis that are between 10g and 20g	<V8min,V8max>
	Number of points on the Y-axis that are between 20g and 30g	<V9min,V9max>
	Number of points on the Y-axis that are between 30g and 40g	<V10min,V10max>
	Number of points on the Y-axis that are between 40g and 50g	<V11min,V11max>
	Number of points on the Y-axis greater than 50g	<V12min,V12max>

Step (3): Import the data into the test matter-element.

Import the data into the test matter-element, as shown in Eq. (6).

$$R_x = \left(q, C_j, X_j\right) = \begin{Bmatrix} q & c_1 & x_1 \\ & c & x_2 \\ & \cdots & \cdots \\ & c_j & x_j \end{Bmatrix} \tag{6}$$

Here, j represents the number of features and q the name of the test object.

Step (4): Calculate the extension distance.

In this step, the distance between the test object x_j and the classical domain was completed as shown in Eq. (7), and the distance between the test object x_j and the universe domain was completed as shown in Eq. (8).

$$\rho\left(x_j, X_{ki}\right) = \left| x_j - \frac{m_{ki} + l_{ki}}{2} \right| - \frac{l_{ki} - m_{ki}}{2} \tag{7}$$

$$\rho\left(x_j, X_{pi}\right) = \left| x_j - \frac{m_{pi} + l_{pi}}{2} \right| - \frac{l_{pi} - m_{pi}}{2} \tag{8}$$

Here, $\rho(x_j, X_{ki})$ represents the distance between the input value x_j and the classical domain, and $\rho(x_j, X_{pi})$ the distance between the input value x_j and the universe domain.

To provide a more intuitive understanding of the relationship between the input value x_j and the universe domain as well as the classical domain, the relationship was represented as shown in Eq. (9).

$$D\left(x_j, X_{ki}, X_{pi}\right) = \begin{cases} \rho\left(x_j, X_{pi}\right) - \rho\left(x_j, X_{ki}\right), & x \notin X_o \\ \dfrac{\left|l_{ki} - m_{ki}\right|}{-2}. & x \in X_o \end{cases} \tag{9}$$

Here, $D(x_j, X_{ki}, X_{pi})$ represents the relationship between the input value and the universe and classical domains. We measure the correlation function between the test matter-element and extension sets of other types, as shown in Eq. (10).

Step (5): Calculate the correlation function.

$$K_k\left(x_j\right) = \begin{cases} 0, & x \le 0 \\ \dfrac{\rho\left(x_j, X_{ki}\right)}{D\left(x_j, X_{ki}, X_{pi}\right)}. & x > 0 \end{cases} \tag{10}$$

Here, $K_k(x_j)$ represents the correlation function for the jth characteristic value of the kth type.

Step (6): Calculate the correlation degree.

Multiply the correlation function by the weight to obtain the correlation degree, as shown in Eq. (11).

$$K_k\left(all\right) = \sum_{j=1}^{n} \omega_j \times K_k\left(x_j\right) \tag{11}$$

Here, $K_k(all)$ represents the correlation function value of the model under test.

Step (7): Normalize the correlation values.

Let $K_k(all)^*$ represent the normalization of the correlation values, keeping the correlation value of each type of set within the interval [−1, 1], as shown in Eq. (12).

$$K_k\left(all\right)^* = \frac{2K_k\left(all\right) - K_k\left(all\right)_{min} - K_k\left(all\right)_{max}}{K_k\left(all\right)_{max} - K_k\left(all\right)_{min}} \tag{12}$$

Step (8): Determine the type of matter-element under test.

After the calculations in step (7), the correlation value for each category was obtained. The test object was classified into the category with the highest value. Then, return to step (3) to continue classifying the next test object.

5. Experimental Results

5.1 Feature extraction results

To identify the types of fault in the gearbox, the vibration signals captured in this study are shown in Figs. 8 and 9.

After filtering, vibration signals of four gearbox models were obtained. Each model had 200 data points for both the *X*- and *Y*-axes, with each data point represented as a 1*51200 vector. On the basis of the features listed in Table 4, the vector was sequentially searched. After processing all the data, the universe and classical domains for each model were set, and the results are shown in Fig. 10.

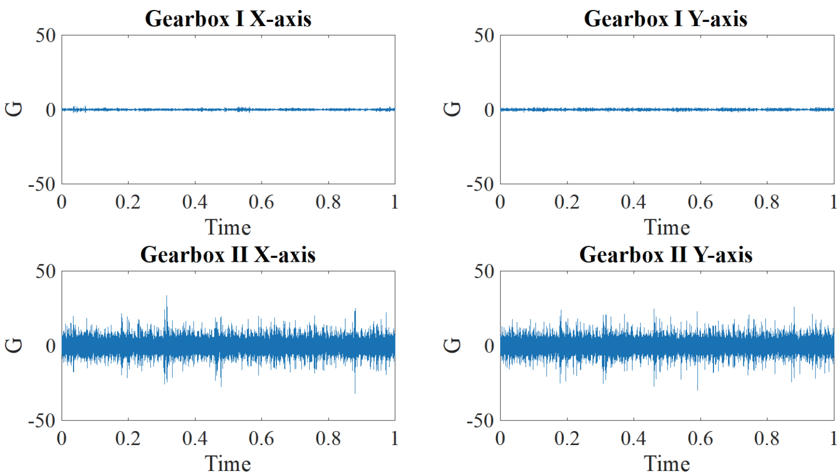

Fig. 8. (Color online) Vibration signals of gearbox I and gearbox II in the article.

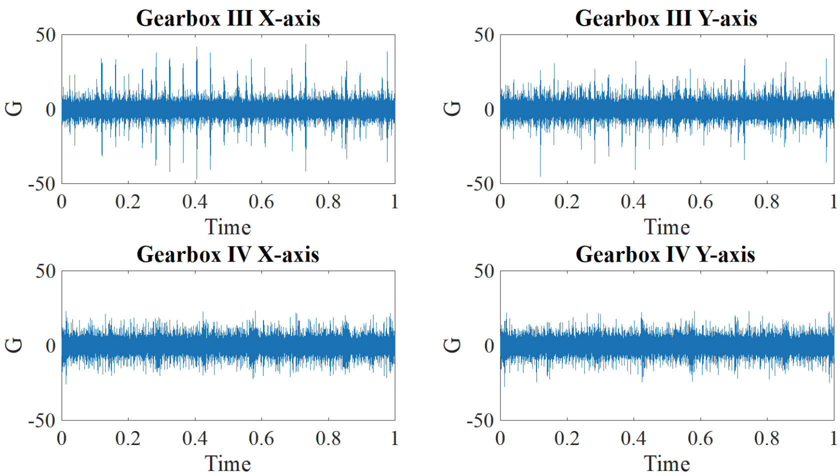

Fig. 9. (Color online) Vibration signals of gearbox III and gearbox IV in the article.

$$\begin{bmatrix} 4.47 & 116.69 \\ 3.38 & 100.93 \\ 0 & 1214 \\ 0 & 218 \\ 0 & 64 \\ 0 & 12 \\ 0 & 3 \\ 0 & 1371 \\ 0 & 101 \\ 0 & 19 \\ 0 & 3 \\ 0 & 1 \end{bmatrix} \quad \begin{bmatrix} 4.47 & 6.5 \\ 3.38 & 5.4 \\ 0 & 0 \\ 0 & 0 \\ 0 & 0 \\ 0 & 0 \\ 0 & 0 \\ 0 & 0 \\ 0 & 0 \\ 0 & 0 \\ 0 & 0 \\ 0 & 0 \end{bmatrix} \quad \begin{bmatrix} 47.17 & 103.17 \\ 49.23 & 76.24 \\ 602 & 1050 \\ 8 & 122 \\ 0 & 26 \\ 0 & 8 \\ 0 & 1 \\ 540 & 933 \\ 7 & 60 \\ 0 & 6 \\ 0 & 2 \\ 0 & 0 \end{bmatrix} \quad \begin{bmatrix} 69.77 & 116.69 \\ 64.51 & 100.93 \\ 682 & 1007 \\ 50 & 218 \\ 2 & 64 \\ 0 & 12 \\ 0 & 3 \\ 921 & 1371 \\ 35 & 101 \\ 0 & 19 \\ 0 & 3 \\ 0 & 1 \end{bmatrix} \quad \begin{bmatrix} 41.31 & 64.65 \\ 43.24 & 57.85 \\ 556 & 1214 \\ 0 & 31 \\ 0 & 3 \\ 0 & 0 \\ 0 & 0 \\ 492 & 915 \\ 1 & 22 \\ 0 & 0 \\ 0 & 0 \\ 0 & 0 \end{bmatrix}$$

(a) (b) (c) (d) (e)

Fig. 10. Universe and classical domains of this paper: (a) universe domain and classical domains of (b) gearbox I, (c) gearbox II, (d) gearbox III, and (e) gearbox IV.

5.2 Identification results

We employed extension correlation functions to compute the identification of fault types. A total of 1600 vibration signals from gearboxes were collected, with 400 samples for each type of data. Among them, 200 samples were utilized for calculating the classical and universe domains in the correlation function, while the remaining 200 samples were used to test the accuracy of the extension detection method.

Common evaluation metrics included accuracy, precision, recall, and $F1$ score. These metrics helped provide a comprehensive assessment of the model's performance in fault classification. The confusion matrix of the extended detection method is shown in Fig 11. The evaluation metrics for the extension detection method are listed in Table 5.

According to the method proposed in this article, the experimental results indicate that the recognition rate reached 94.625%.

6. Discussion

The proposed method demonstrated the potential of the extension detection method in wind turbine gearbox applications. Owing to the characteristics of the extension set, which ranges from $-\infty$ to $+\infty$,[23] quantifying feature values was easier, and recognition could be performed without converting the measured data into images, saving a significant amount of time; however, it required manually setting many parameters.

Artificial intelligence algorithms (such as neural networks or long short-term memory networks) had the ability to adjust parameters automatically. Deep learning models, in particular, could learn data features autonomously, reducing the need for manual parameter settings.[19–21]

The extension detection method performed excellently in scenarios with a smaller number of samples and clear fault characteristics, making it especially suitable for data containing ambiguity, nonlinearity, and variable parameters. However, as the data volume increased or the

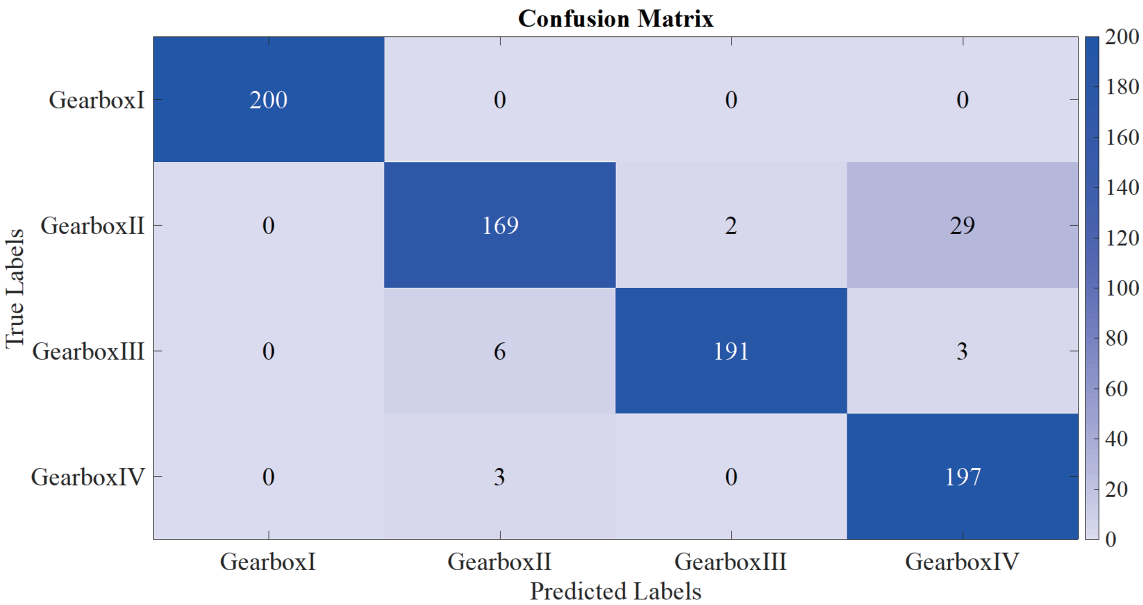

Fig. 11. (Color online) Confusion matrix of the extended detection method.

Table 5
Evaluation metrics of the extended detection method.

Accuracy	Precision	Recall	*F*1 score
94.625%	94.98%	94.62%	94.62%

feature space became more complex, the workload and difficulty of parameter setup increased significantly.

In contrast, AI technology had greater advantages in situations with large data volumes, automated requirements, and unpredictable parameters. Particularly when fault data contained implicit nonlinear characteristics, AI technology could automatically learn and extract deep patterns from the data. Furthermore, AI's transfer learning capability allowed models to adapt and be deployed quickly in new scenarios, whereas the extension detection method required additional parameter adjustments. On the basis of the strengths and weaknesses of both methods, future research could consider combining the extension detection method with AI technology.

7. Conclusions

The method proposed in this article utilizes vibration signals from a gearbox, which undergo FFT. On the basis of their peak-to-peak values and the number of points generated at specific intervals, these signals are used as features for calculating the extension correlation functions, aiming to achieve fault identification. The method effectively identifies gearbox faults in wind turbine generators under different conditions, achieving a recognition rate of 94.625%. By simply filtering the raw data, the correlation function calculation can be directly performed without the need for extensive data processing, thus enabling the efficient fault identification of the wind turbine gearbox.

References

1 S. Paul, T. Dey, P. Saha, S. Dey, and R. Sen: Proc. 2021 Innovations in Energy Management and Renewable Resources (IEEE, 2021) 1–2. https://doi.org/10.1109/IEMRE52042.2021.9386748
2 F. Ayadi, I. Colak, I. Garip, and H. I. Bulbul: Proc. 2020 8th Int. Conf. Smart Grid (icSmartGrid) (IEEE, 2020) 183–188. https://doi.org/10.1109/icSmartGrid49881.2020.9144695
3 H. Zhang, S. Li, and H. Sun: Math. **12** (2024) 1410. https://doi.org/10.3390/math12091410
4 H. Liu, J. Zhang, Y. Cheng, and C. Lu: J. Sound Vib. **385** (2016) 350. https://doi.org/10.1016/j.jsv.2016.09.005
5 T. Wang, Q. Han, F. Chu, and Z. Feng: Mech. Syst. Signal Process. **126** (2019) 662. https://doi.org/10.1016/j.ymssp.2019.02.051
6 L. Wang, Y. Shao, and Z. Cao: Measurement **125** (2018) 554. https://doi.org/10.1016/j.measurement.2018.05.023
7 J. Chen, D. Zhou, C. Lyu, and C. Lu: Mech. Syst. Signal Process. **113** (2018) 102. https://doi.org/10.1016/j.ymssp.2017.08.010
8 G. L. McDonald, Q. Zhao, and M. J. Zuo: Mech. Syst. Signal Process. **33** (2012) 237. https://doi.org/10.1016/j.ymssp.2012.06.010
9 Z. Li, Y. Jiang, C. Hu, and Z. Peng: Measurement **90** (2016) 4. https://doi.org/10.1016/j.measurement.2016.04.036
10 Z. Wang, H. Wang, and W. Liu: Proc. 2018 IEEE 15th Int. Conf. e-Business Engineering (ICEBE, 2018) 234–238. https://doi.org/10.1109/ICEBE.2018.00045
11 Y.-P. Huang and H.-J. Chen: Proc. Engineering Solutions for the Next Millennium. 1999 IEEE Canadian Conf. Electrical and Computer Engineering (Cat. No.99TH8411) (IEEE, 1999) 997–982. https://doi.org/10.1109/CCECE.1999.808168
12 W. Zeng, J. Ni, W. Xu, S. Du, and S. Ye: Proc. 2022 4th Int. Conf. Electrical Engineering and Control Technologies (CEECT) (IEEE, 2022) 444–449. https://doi.org/10.1109/CEECT55960.2022.10030688
13 X. Wu, Q. Zhang, X. Chen, and D. Wang: Proc. 2021 IEEE Sustainable Power and Energy Conf. (iSPEC) (IEEE, 2021) 1772–1777. https://doi.org/10.1109/iSPEC53008.2021.9736078
14 D. Zhao, Z. Tang, J. Wang, Z. Han, F. Sun, D. He, and Q. Chen: IEEE Trans. Eng. Manage. **71** (2024) 8488. https://doi.org/10.1109/TEM.2024.3388578
15 Z. Liu, J. Liu, J. Lyu, H. Zhao, and Y. Xu: Alexandria Eng. J. **60** (2021) 2607. https://doi.org/10.1016/j.aej.2020.12.057
16 X. Chen, L. Xu, X. Li, and L. Cong: IEEE Access **12** (2023) 47581. https://doi.org/10.1109/ACCESS.2023.3346678
17 C. Gu, J. Zhu, D. Huang, and X. Wang: Proc. 2020 IEEE 9th Data Driven Control and Learning Systems Conf. (DDCLS) (IEEE, 2020) 1098–1102. https://doi.org/10.1109/DDCLS49620.2020.9275250
18 L. Cao, J. Zhang, J. Wang, and Z. Qian: Proc. 2019 IEEE 28th Int. Symp. Industrial Electronics (ISIE) (IEEE, 2019) 890–895. https://doi.org/10.1109/ISIE.2019.8781108
19 A. Amin, A. Bibo, M. Panyam, and P. Tallapragada: Proc. 2022 American Control Conf. (ACC) (IEEE, 2022) 3777–3782. https://doi.org/10.23919/ACC53348.2022.9867477
20 J. He, Ping Wu, J. Gao, X. Zhang, and S. Lou: Proc. 2020 7th Int. Conf. Inf. Cybernetics and Computational Social Systems (ICCSS) (IEEE, 2020) 517–521. https://doi.org/10.1109/ICCSS52145.2020.9336913
21 S. Zhang, T. Shan, Z. You, Z. Jie, L. Cao, and J. Wang: Proc. 2024 IEEE Int. Conf. Sensing, Diagnostics, Prognostics, and Control (SDPC) (IEEE, 2024) 52–56. https://doi.org/10.1109/SDPC62810.2024.10707732
22 K. H. Chao, R. H. Lee, and K. L. Yen: 2008 Int. Conf. Machine Learning and Cybernetics (IEEE, 2008) 1882–1887. https://doi.org/10.1109/ICMLC.2008.4620713
23 C. Y. Yang: 2007 Int. Conf. Wavelet Analysis and Pattern Recognition (IEEE, 2007) 819–824. https://doi.org/10.1109/ICWAPR.2007.4420782

About the Authors

Meng-Hui Wang received his M.S. degree in electrical engineering in 1990 and his Ph.D. degree in the same field in 1994, both from National Taiwan University of Science and Technology. He came to National Chin-Yi University of Technology (NCUT) in August 1994 and is now affiliated with the Department of Electrical Engineering as a lifetime distinguished professor. His major areas of research include renewable energy systems, power systems, extension theory, and AI applications. He is a member of the Chinese Association of Artificial Intelligence (CAAI), the vice president of the Taiwan Education Society of Innovation & Invention (TESII), and the chairman of the 6th Intelligent Living Technology Association of Taiwan (ILTAT). He was the general chair of the 1st Intelligent Living Technology Conference (2006) and the honorary co-chair of the 2012 International Symposium on Computer, Consumer, and Control (IS3C). (wangmh@ncut.edu.tw)

Yu-Xian Su received his B.S. degree from the Department of Electrical Engineering, National Chin-Yi University of Technology, Taichung City, Taiwan, in 2024. His main research interests include wind turbines and fault diagnosis. (a0906022998@gmail.com)

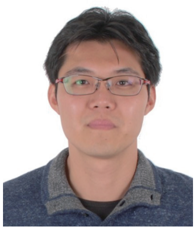

Shiue-Der Lu received his M.S. degree from Chung Yuan Christian University, Taoyuan City, Taiwan, in 2006 and his Ph.D. degree from the National Taiwan University of Science and Technology, Taipei City, Taiwan, in 2013, both in electrical engineering. From 2012 to 2016, he was a researcher at the Industrial Technology Research Institute. From 2016 to 2018, he was an assistant researcher at the Department of Electrical Engineering, Chung Yuan Christian University. Since 2018, he has been with the Department of Electrical Engineering, National Chin-Yi University of Technology, Taichung City, Taiwan, where he is currently an associate professor. He is also the secretary-general of the 6th Intelligent Living Technology Association of Taiwan (ILTAT). His research interests include renewable energy, power quality, the damage diagnosis of wind power generators, and artificial intelligence applications in power systems. (sdl@ncut.edu.tw)